arXiv:1608.00083v1 [cond-mat.stat-mech] 30 Jul 2016

Magnon-bound-state hierarchy for the two-dimensional transverse-field Ising model in the ordered phase

Yoshihiro Nishiyama

Department of Physics, Faculty of Science, Okayama University, Okayama 700-8530, Japan

Abstract

In the ordered phase for an Ising ferromagnet, the magnons are attractive to form a series of bound states with the mass gaps, $m_2 < m_3 < \ldots$. Each ratio $m_{2,3,\ldots}/m_1$ (m_1: the single-magnon mass) is expected to be a universal constant in the vicinity of the critical point. In this paper, we devote ourselves to the $(2+1)$-dimensional counterpart, for which the universal hierarchical character remains unclear. We employed the exact diagonalization method, which enables us to calculate the dynamical susceptibility via the continued-fraction expansion. Thereby, we observe a variety of signals including $m_{2,3,4}$, and the spectrum is analyzed with the finite-size-scaling method to estimate the universal mass-gap ratios.

Keywords:
05.50.+q 05.10.-a 05.70.Jk 64.60.-i

1. Introduction

For an Ising ferromagnet in the ordered phase, the magnons are attractive, forming a series of bound states with the mass gaps, $m_2 < m_3 < \ldots$. As a matter of fact, in $(1+1)$ dimensions, where the system is integrable [1], there exist eight types of elementary excitations with the universal mass gaps

$$\begin{aligned} m_2/m_1 &= 2\cos\pi/5 \\ m_3/m_1 &= 2\cos\pi/30 \\ m_4/m_1 &= 4\cos\pi/5\cos 7\pi/30 \\ m_5/m_1 &= 4\cos\pi/5\cos 2\pi/15 \\ m_6/m_1 &= 4\cos\pi/5\cos\pi/30 \end{aligned}$$

$$
\begin{aligned}
m_7/m_1 &= 8\cos^2\pi/5\cos 7\pi/30 \\
m_8/m_1 &= 8\cos^2\pi/5\cos 2\pi/15,
\end{aligned}
$$

(m_1: single-magnon mass gap) in the vicinity of the critical point [2, 3]. According to the rigorous theory, the *elementary* magnon m_1 is also a composite particle, reflecting a highly non-perturbative character of this problem; in this sense, the underlying physics may lie out of the conventional "magnon" picture. Experimentally, the lowest one $m_2/m_1 = 1.618\ldots$ (golden ratio) was observed [4] for a quasi-one-dimensional quantum Ising ferromagnet, $CoNb_2O_6$ [5, 6]. Above $\omega/m_1 \geq 2$, there extends a two-magnon continuum, overwhelming fine details of the spectrum; see Fig. 4 E of Ref. [4], for instance.

In $(2+1)$ dimensions, on the contrary, such rigorous information is not available, and details of the bound-state hierarchy are not fully clarified; the role of dimensionality was argued in §5 of Ref. [10] (see Ref. [13] as well). To the best of author's knowledge, the second-lowest bound state $m_3/m_1 = 2.45(10)$ was detected with the Monte Carlo method [7], whereas the lowest one, $m_2/m_1 \approx 1.81$ [8], has been investigated rather extensively so far [7, 9, 10, 11, 12, 13]. In this paper, we investigate the $(2+1)$-dimensional Ising model (1) with the exact diagonalization method, which enables us to calculate the dynamical susceptibility via the continued-fraction expansion [14]; note that in the Monte Carlo simulation, one has to resort to the inverse Laplace transform to obtain the spectrum. The spectrum reflects a hierarchical character for $m_{2,3,\ldots}$. In Fig. 1, we present a schematic drawing for a spectral function within the zero-momentum sector.

It has to be mentioned that the magnon-bound-state hierarchy is relevant to the glueball spectrum (screening masses) for the gauge field theory (Svetitsky-Yaffe conjecture) [15, 16, 17]. Actually, we show that in the next section, the bound-state hierarchy $m_{2,3,4}$ bears a resemblance to the glueball spectrum for the Z_2-symmetric gauge field theory [16]. Here, we dwell on the characterization of the magnon bound states, and the verification of the conjecture itself lies beyond the scope of this paper.

To be specific, we present the Hamiltonian for the two-dimensional spin-$S = 1$ transverse-field Ising model

$$
\mathcal{H} = -J\sum_{\langle ij\rangle} S_i^z S_j^z - J'\sum_{\langle\langle ij\rangle\rangle} S_i^z S_j^z - J_4\sum_{\langle ij\rangle}(S_i^z S_j^z)^2
$$

$$-J_4' \sum_{\langle\langle ij \rangle\rangle} (S_i^z S_j^z)^2 + D \sum_i (S_i^z)^2 - \Gamma \sum_i S_i^x - H \sum_i S_i^z, \qquad (1)$$

with the quantum spin-$S = 1$ operator $\mathbf{S}_i$ placed at each square-lattice point i. The summations, $\sum_{\langle ij \rangle}$ and $\sum_{\langle\langle ij \rangle\rangle}$, run over all possible nearest-neighbor and next-nearest-neighbor pairs, $\langle ij \rangle$ and $\langle\langle ij \rangle\rangle$, respectively. Correspondingly, J (J_4) and J' (J_4') are the quadratic (biquadratic) interaction parameters. The symbols, D, Γ and H, denote the single-ion anisotropy, the transverse- and longitudinal-magnetic fields, respectively. The parameter D is tunable, and the phase diagram is presented in Fig. 2. Other interaction parameters are set to

$$\begin{aligned} (J, J', J_4, J_4', \Gamma) &= [0.41191697085, 0.16125069616, -0.11764020018, \\ &\quad -0.05267926601, 1.0007], \end{aligned} \qquad (2)$$

so as to suppress corrections to scaling [18]. The (properly scaled) infinitesimal magnetic field $H = 11L^{-y_h}$ [18] with $y_h = 2.481865$ [19] resolves the ground-state two-fold degeneracy [3]. The $S = 1$-spin model permits us to incorporate extended interactions so as to suppress corrections to scaling [20]. In fact, as demonstrated in Ref. [18], even for restricted system sizes, the Hamiltonian (1) exhibits suppressed corrections to scaling. Detailed account of the three-dimensional Ising universality is reported in Ref. [19].

The rest of this paper is organized as follows. In Sec. 2, we present the numerical results. The simulation algorithm is explained as well. In Sec. 3, we address the summary and discussions.

2. Numerical results

In this section, we present the numerical results for the (2+1)-dimensional Ising model (1). We employed the exact diagonalization method for the finite-size cluster with $N \leq 22$ spins. We imposed the screw-boundary condition [21] to treat an arbitrary number of spins $N = 16, 18, \ldots$. We adopt the simulation algorithm presented in Appendix of Ref. [18]. Because the N spins constitute a rectangular cluster, the linear dimension of the cluster is given by the formula

$$L = \sqrt{N}. \qquad (3)$$

The diagonalization was performed within the zero-momentum subspace.

2.1. *Critical behavior of the single-magnon mass gap m_1*

In this section, we make a finite-size-scaling analysis for the single-magnon mass gap m_1, which sets a fundamental energy scale in the subsequent scaling analyses. The single-magnon mass m_1 corresponds to the first excitation gap above the ground state. (The ground-state two-fold degeneracy is resolved by H, as mentioned in Sec. 1.)

In Fig. 3, we present the scaling plot, $(D - D_c)L^{1/\nu}$-Lm_1, for the number of spins, (+) $N = 16$, (×) 18, (∗) 20, and (□) 22. Here, the scaling parameters, $D_c = -0.39781956122$ and $\nu = 0.63002$, are taken from the existing literatures, Refs. [18] and [19], respectively. That is, there is no adjustable fitting parameter in the scaling analysis. We observe that the data in Fig. 3 collapse into a scaling curve for a considerably wide range of the parameter D. The simulation data already enter the scaling regime. Encouraged by this finding, we turn to the analysis of the spectral properties.

Last, we address a few remarks. First, the data in Fig. 3 indicate that the gap closes beside the critical point, and the gap itself seems to be rather large. These confusing features are due to the infinitesimal (scaled) longitudinal magnetic field as mentioned in Introduction. This infinitesimal magnetic field resolves the ground-state degeneracy, stabilizing the magnetic excitations [18]. Last, right at the critical point, the excitation hierarchy becomes smeared out. The smearing-out regime extends within a bound $|D - D_c| \propto 1/L^{1/\nu}$, which shrinks in the thermodynamic limit.

2.2. *Finite-size-scaling analysis of the dynamical susceptibility $\chi''_{Y^2}(\omega)$: Magnon-bound-state hierarchy*

In this section, we investigate the magnon-bound-state hierarchy. For that purpose, we introduce the dynamical susceptibility

$$\chi''_{Y^2}(\omega) = -\Im\langle 0|M^\dagger_{Y^2}(\omega - \mathcal{H} + E_0 + \mathrm{i}\eta)^{-1}M_{Y^2}|0\rangle, \tag{4}$$

with the perturbation operator

$$M_{Y^2} = \mathcal{P}\left(\sum_{i=1}^{N} S^y_i\right)^2, \tag{5}$$

and the projection operator $\mathcal{P} = 1 - |0\rangle\langle 0|$. Here, the symbols, η and E_0 ($|0\rangle$), denote the energy-resolution parameter and the ground-state energy (vector), respectively. The dynamical susceptibility was calculated with the

continued-fraction expansion [14]. Rather technically, the continued-fraction expansion requires the iteration sequences less than those of the Lanczos diagonalization for E_0 and $|0\rangle$; namely, at least for drawing the spectra such as Fig. 4-7, the results converge rapidly possibly owing to the plausible choice of M_{Y^2}. The dynamical susceptibility obeys [22] the scaling formula

$$\chi''_{Y^2} = L^5 g(\omega/m_1, (D - D_c)L^{1/\nu}), \tag{6}$$

with a scaling function g. Afterward, the power-law singularity $\sim L^5$ as well as the physical content of χ_{Y^2} are considered.

In Fig. 4, we present the scaling plot, ω/m_1-$L^{-5}\chi''_{Y^2}$, with fixed $(D - D_c)L^{1/\nu} = -17$ and $\eta = 0.1m_1$ for various $N = 18$ (dotted), 20 (solid), and 22 (dashed). The scaling parameters, D_c and ν, are the same as those of Fig. 3. The curves in Fig. 4 collapse into a scaling function g, Eq. (6), indicating that the simulation data already enter the scaling regime.

The peaks in Fig. 4 reflect a universal character of the magnon excitations in proximity to the critical point; see a schematic drawing, Fig. 1, as well. The peaks at $\omega/m_1 \approx 1$, 1.8, 2, 2.5 and 3 correspond to the m_1, m_2 [7, 8, 10, 11, 12, 13], $2m_1$ (two-magnon-continuum threshold), m_3 [7], and m_4 excitations, respectively. The $\omega/m_1 \approx 4.8$-peak may be attributed to either a yet higher bound state m_5 or a composite particle made of m_2 and $2m_1$.

It has to be mentioned that these excitations $m_{2,3,4}$ correspond to the glueball spectrum (screening masses) for the gauge field theory (Svetitsky-Yaffe conjecture [15]). For instance, according to the Monte Carlo simulation of the Z_2 lattice gauge-field theory [16], there appear a variety of particles (the so-called glueballs), $m_{(0^+)'}/m_{0^+} = 1.88(2)$, $m_{(0^+)''}/m_{0^+} = 2.59(4)$, and $m_{(0^-)}/m_{0^+} = 3.25(16)$, quite reminiscent of the above-mentioned $m_{2,3,4}/m_1$, respectively; here we follow the notation of Ref. [16]. Our simulation result supports the Svetitsky-Yaffe conjecture at least up to m_4.

A few remarks are in order. First, we consider the power-law singularity of $\chi_{Y^2} \sim L^5$, Eq.(6). By analogy to the random-walk translation distance, the singularity of the perturbation operator $M_{Y^2} = (\sum_{i=1}^{N} S_i^y)^2$, Eq. (5), is counted as $\sim N(= L^2)$. On the one hand, the reciprocal energy gap should exhibit the singularity, $(\omega - \mathcal{H} + E_0 + \mathrm{i}\eta)^{-1} \sim L$. These formulas lead to $\chi''_{Y^2} \sim L^5$. As a matter of fact, there also appears a non-trivial term $\chi_{Y^2} \sim L^{2/\nu-3}$; this term is less singular than the above $\sim L^5$, and it was dropped in Eq. (6). Here, a key ingredient is that an infinitesimal y-direction magnetic field H^y is perpendicular to Γ, and hence, the scaling

dimension of H^y is a half of Γ. Second, we make an overview of the dynamical susceptibilities appearing in literature. So far, there have been utilized two types of perturbations, namely, off-diagonal $M_Y = \sum_{i=1}^{N} S_i^y$ and diagonal $M_Z = \sum_{i=1}^{N} S_i^z$ ones, in the course of study for both $(1+1)$- and $(2+1)$-dimensional systems. The former M_Y was employed in Refs. [23, 24, 25, 26]. Our choice M_{Y^2} (5) is based on these elaborated studies. We found that the duplicated operations $(M_Y)^2 = M_{Y^2}$ create the $m_{3,4}$ particles more efficiently than a mere M_Y, at least, for the $(2+1)$-dimensional counterpart. The latter M_Z was implemented in Refs. [25, 26, 27]. This choice leads to the ordinary uniform magnetic AC susceptibility, and it is of experimental significance. Last, we mention the parameter setting of the peak-broadening factor η. In this paper, aiming to avoid *ad hoc* adjustment of η, we fixed the value of η throughout the study. The continuum spectrum in Fig. 7 seems to be well reproduced by this setting.

2.3. Universality of the bound-state hierarchy $m_{2,3,4}/m_1$

In the above section, through the probe χ''_{Y^2}, we resolved the $m_{2,3,4}$ signals out of the two-magnon continuum. In this section, we examine the universality of each mass-gap ratio $m_{2,3,4}/m_1$ with respect to the variation of $(D - D_c)L^{1/\nu}$.

In Fig. 5, we present the scaling plot, ω/m_1-$L^{-5}\chi''_{Y^2}$, with $N = 22$ and $\eta = 0.1m_1$ for various values of the scaling argument, $(D - D_c)L^{1/\nu} = -15$ (dashed), -17 (solid), and -19 (dotted); here, the scaling parameters, D_c and ν, are the same as those of Fig. 3. Note that the curves do not necessarily overlap, because the scaling argument $(D - D_c)L^{1/\nu}$ is ranging; see Eq. (6). In fact, the m_2-peak heights do not coincide each other, whereas the peak position, $m_2/m_1 \approx 1.81$ [8], appears to be kept invariant with $(D - D_c)L^{1/\nu}$ varied. Our result supports the universality of $m_2/m_1 \approx 1.81$ [8], which has been established in the course of study [7, 10, 11, 12, 13].

We turn to the analysis of the second-lowest bound state, m_3/m_1. In Fig. 5, we observe that the peak position m_3/m_1 is kept invariant with $(D - D_c)L^{1/\nu}$ varied. In closer look ($N = 22$), the peak positions read $m_3/m_1 \approx 2.56$, 2.55, and 2.56 for $(D - D_c)L^{1/\nu} = -15$, -17, and -19, respectively. Namely, the condition $(D - D_c)L^{1/\nu} = -17$ is an optimal one in the sense that the peak position m_3/m_1 takes a stable (extremal) value

$$m_3/m_1 = 2.55. \tag{7}$$

Our result agrees with the Monte Carlo result $m_3/m_1 = 2.45(10)$ [7].

Additionally, we are able to appreciate the universal intrinsic peak width for m_3. The m_3 particle may decay into a pair of m_1, and eventually, the peak acquires a finite life time, namely, a reciprocal intrinsic peak width; because the $(2+1)$-dimensional system is not integrable, it is natural that the spectral intensities are diffused [25]. In Fig. 6, we present the scaling plot, ω/m_1-$L^{-5}\chi''_{Y^2}$, with $(D-D_c)L^{1/\nu} = -5.5$ and $\eta = 0.1m_1$ for $N = 18$ (dotted), 20 (solid), and 22 (dashed); the scaling parameters, D_c and ν, are the same as those of Fig. 3. In this scaling regime, $(D-D_c)L^{1/\nu} = -5.5$, the m_3 peak splits into two sub-peaks at $\omega/m_1 \approx 2.41$ and 2.65 ($N = 22$). The distance between these sub-peaks provides an indicator for the intrinsic peak width

$$\delta m_3/m_1 = 0.24. \tag{8}$$

The peak width is smaller by one order of magnitude than the mass (7), indicating that the m_3 particle is a stable collective mode, and it would be observable experimentally. We consider that the error margin for $m_3/m_1 = 2.55$, Eq. (7), would not exceed a half of this peak width; namely, the uncertainty for $m_3/m_1 = 2.55$, Eq. (7), is bounded by 0.12.

Last, we consider the m_4 signal. From Fig. 5, we estimate the mass-gap ratio as $m_4/m_1 \approx 3$. The peak position appears to drift, indicating that this peak consists of diffused intensities. In fact, there are a number of decay modes such as $m_4 \to 2m_1$, $m_1 + m_2$ and $3m_1$, giving rise to a considerably broadened line shape as to m_4. Further details are not fixed by the available result.

We address a remark on the D-dependence of the spectrum. As mentioned above, the peak position takes a stable (extremal) value at an optimal condition $(D-D_c)L^{1/\nu} = -17$. In a closer look, however, there are irregularities caused by the level crossing. A level-crossing point locates at the above-mentioned point $(D-D_c)L^{1/\nu} = -5.5$, and another one occurs around $(D-D_c)L^{1/\nu} = -14$, where the data of $N = 20$ and 22 are not very influenced. In this sense, these intermittent irregularities are due to the finite-size artifact, reflecting the fact that the bound state is embedded within the continuum. As mentioned above, the level crossing provides information how the spectral intensity is distributed over the discrete levels, and hence, it indicates the intrinsic peak width of the spectral peak concerned. Nevertheless, apart from these intermittent irregularities, the peak position is kept invariant for a considerably wide range of D, and the slight wavy deviation appears to be bounded by the above-mentioned error margin.

2.4. Finite-size-scaling analysis of the dynamical susceptibility $\chi''_{z^2}(\omega)$: Two-magnon continuum

In this section, we investigate the dynamical susceptibility χ''_{z^2}, Eq. (9); here, the perturbation operator M_{z^2} (10) is identical to the D term of the Hamiltonian (1), and such a dynamical susceptibility is called the scalar susceptibility [22] in literature.

In Fig. 7, we present the scaling plot, ω/m_1-$L^{-2/\nu+1}\chi''_{z^2}$, with $(D - D_c)L^{1/\nu} = -17$ and $\eta = 0.1m_1$ for $N = 18$ (dotted), 20 (solid), and 22 (dashed); the scaling parameters, D_c and ν, are the same as those of Fig. 3. The dynamical susceptibility is defined by the formula

$$\chi''_{z^2}(\omega) = -\Im\langle 0|M^\dagger_{z^2}(\omega - \mathcal{H} + i\eta)^{-1}M_{z^2}|0\rangle, \tag{9}$$

with the perturbation operator

$$M_{z^2} = \mathcal{P}\sum_{i=1}^{N}(S^z_i)^2. \tag{10}$$

The dynamical susceptibility obeys the scaling law $\chi''_{z^2} = L^{2/\nu-1}h(\omega/m_1, (D-D_c)L^{1/\nu})$ [22] with a scaling function h.

The data in Fig. 7, indicate that this probe χ''_{z^2} is sensitive to the two-magnon continuum, particularly, its threshold $\omega/m_1 \approx 2$. Actually, in contrast to Fig. 4, the bound-state hierarchy $m_{3,4}$ becomes invisible instead. Our simulation result suggests that the choice of the perturbation operator is vital to the detection of the bound-state hierarchy.

We address a remark. The scatter of the scaling curves in Fig. 7 should be attributed to the regular part (non-singular contribution) of χ''_{z^2}. Because the leading singularity of $\chi''_{z^2} \sim L^{2/\nu-1}$ is rather weak, it is contaminated by such residual scaling corrections.

3. Summary and discussions

The universal character of the magnon-bound-state hierarchy for the two-dimensional quantum Ising model (1) in the ordered phase was investigated. So far, the lowest bound state m_2 has been investigated rather extensively [7, 8, 9, 10, 11, 12, 13]. We employed the exact diagonalization method, which yields the dynamical susceptibilities χ''_{Y^2,z^2} via the continued-fraction expansion [14]. The dynamical susceptibility χ''_{Y^2} resolves the bound-state

hierarchy $m_{2,3,4}$ out of the two-magnon continuum. Making the finite-size-scaling analysis of χ''_{Y^2}, we estimated the mass-gap ratios. The lowest one agrees with the preceding result $m_2/m_1 = 1.81$ [8], which has been established in the course of study [7, 10, 11, 12, 13]. For the second-lowest bound state, we estimated the mass-gap ratio, $m_3/m_1 = 2.55$. Our result agrees with the Monte Carlo result $m_3/m_1 = 2.45(10)$ [7]. Additionally, we appreciated its intrinsic peak width, $\delta m_3/m_1 = 0.24$; the bound state m_3 exhibits a rather long life time as a stable collective mode, though it is embedded within the continuum. A signature for the third-lowest bound state is also detected around $m_4/m_1 \approx 3$. In contrast to χ''_{Y^2}, the probe χ''_{z^2} is sensitive to the two-magnon continuum, which smears out the $m_{3,4}$ signals eventually. The choice of the perturbation field may be significant for resolving the magnon bound states out of the continuum.

As demonstrated in Sec. 2.3, the bound state hierarchy $m_{2,3,4}$ bears a resemblance to the glueball spectrum $m_{(0^+)',(0^+)'',(0^-)}$ [16], supporting the Svetitsky-Yaffe conjecture [15]. It is tempting to apply the similar approach to the q-state Potts model in order to examine the validity of the conjecture. This problem is left for the future study.

Acknowledgment

This work was supported by a Grant-in-Aid for Scientific Research (C) from Japan Society for the Promotion of Science (Grant No. 25400402).

References

[1] A.B. Zamolodchikov, Int. J. Mod. Phys. A **3** (1988) 743.

[2] G. Delfino, J. Phys. A **37** (2004) R45.

[3] P. Fonseca and A. Zamolodchikov, J. Stat. Phys. **110** (2003) 527.

[4] R. Coldea, D. A. Tennant, E. M. Wheeler, E. Wawrzynska, D. Prabhakaran, M. Telling, K. Habicht, P. Smeibidl, and K. Kiefer, Science **327** (2010) 177.

[5] SungBin Lee, R. K. Kaul and L. Balents, Nature Phys. **6** (2010) 702.

[6] N. Ishimura and H. Shiba, Prog. Theor. Phys. **63** (1980) 743.

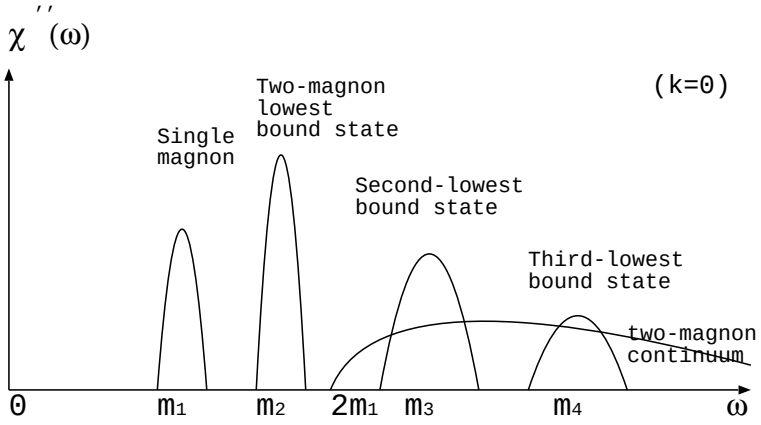

Figure 1: A schematic drawing of the spectral function for the $(2+1)$-dimensional Ising model in the ordered phase at the zero-momentum $k = 0$ sector is shown. The spectrum is expected to exhibit a universal character in the vicinity of the critical point. The m_1 peak corresponds to the single-magnon excitation. The peaks at $m_{2,3,\ldots}$ are the bound states, which may be embedded within the two-magnon continuum extending above $2m_1$.

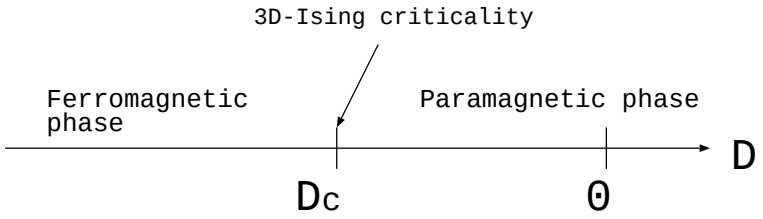

Figure 2: The phase diagram for the two-dimensional transverse-field Ising model (1) is presented; here, the single-ion anisotropy D is a variable parameter, and the other interaction parameters are set to Eq. (2) so as to suppress corrections to scaling [18]. As the parameter D varies, a phase transition separating the ferromagnetic and paramagnetic phases takes place at $D = D_c$.

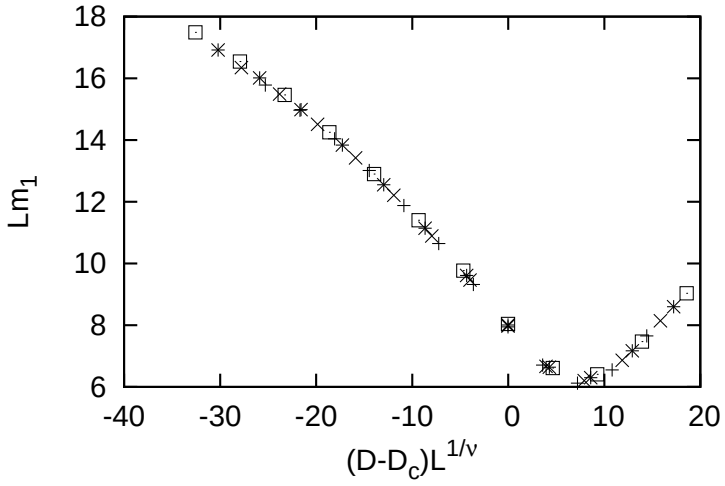

Figure 3: The scaling plot, $(D - D_c)L^{1/\nu}$-Lm_1, is presented for (+) $N = 16$, (×) 18, (∗) 20, and (□) 22. Here, the scaling parameters, $D_c = -0.39781956122$ and $\nu = 0.63002$, are taken from Refs. [18] and [19], respectively; namely, there is no adjustable fitting parameter involved in the scaling analysis.

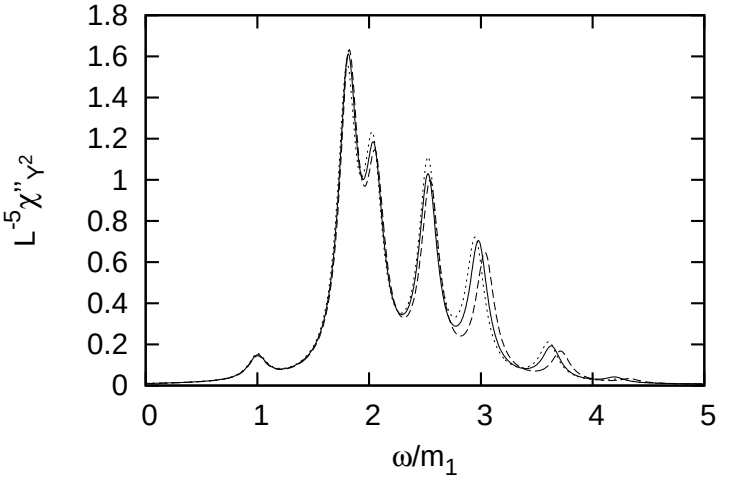

Figure 4: The scaling plot, ω/m_1-$L^{-5}\chi''_{Y^2}(\omega)$, is shown with $(D - D_c)L^{1/\nu} = -17$ and $\eta = 0.1m_1$ for $N = 18$ (dotted), 20 (solid), and 22 (dashed). The scaling parameters, D_c and ν, are the same as those of Fig. 3. The character of each spectral peak is argued in the text.

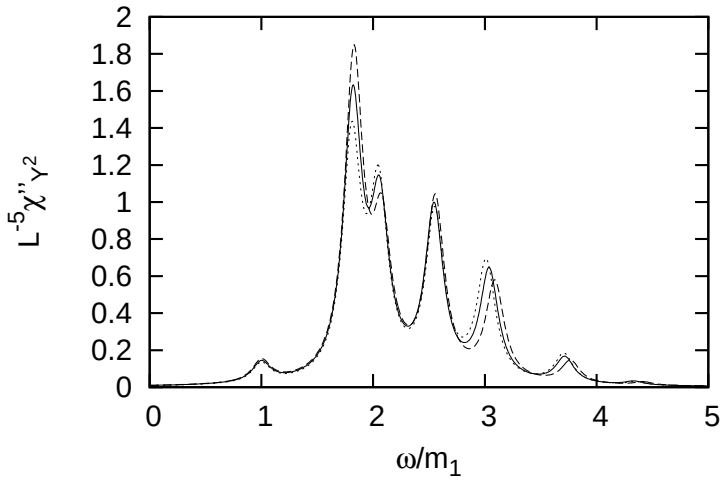

Figure 5: The scaling plot, ω/m_1-$L^{-5}\chi''_{Y^2}(\omega)$, is shown with $N = 22$ and $\eta = 0.1m_1$ for various values of the scaling argument, $(D - D_c)L^{1/\nu} = -15$ (dashed), -17 (solid), and -19 (dotted); the scaling parameters, D_c and ν, are the same as those of Fig. 3. These curves by no means overlap, because the scaling argument is ranging; the heights of the m_2 peak are scattered, whereas the position $m_2/m_1 \approx 1.8$ is kept invariant.

[7] M. Caselle, M. Hasenbusch, and P. Provero, Nucl. Phys. B **556** (1999) 575.

[8] S. Dusuel, M. Kamfor, K. P. Schmidt, R. Thomale, and J. Vidal, Phys. Rev. B **81** (2010) 064412.

[9] D. Lee, N. Salwen, and M. Windoloski, Phys. Lett. B **502** (2001) 329.

[10] M. Caselle, M. Hasenbusch, P. Provero, and K. Zarembo, Nucl. Phys. B **623** (2002) 474.

[11] Y. Nishiyama, Phys. Rev. E **77** (2008) 051112.

[12] Y. Nishiyama, Physica A **413** (2014) 577.

[13] F. Rose, F. Benitez, F. Léonard, and B. Delamotte, arXiv:1604.05285.

[14] E. R. Gagliano and C. A. Balseiro, Phys. Rev. Lett. **59** (1987) 2999.

[15] B. Svetitsky and L. G. Yaffe, Nucl. Phys. B **210** (1982) 423.

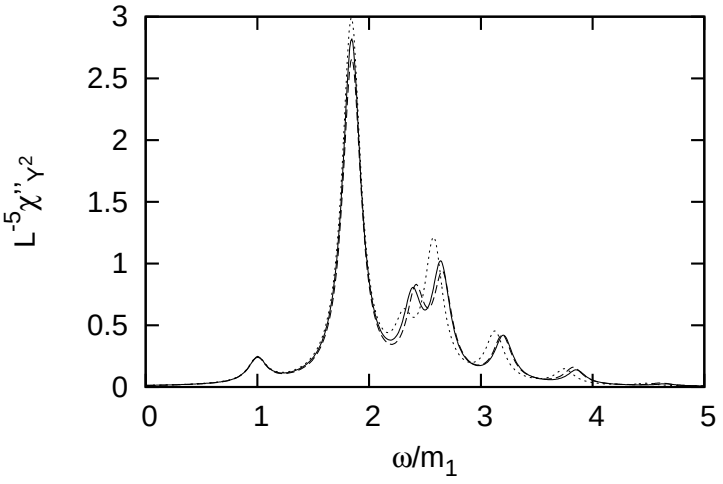

Figure 6: The scaling plot, ω/m_1-$L^{-5}\chi''_{Y^2}(\omega)$, is shown with $(D-D_c)L^{1/\nu}=-5.5$ and $\eta=0.1m_1$ for $N=18$ (dotted), 20 (solid), and 22 (dashed); the scaling parameters, D_c and ν, are the same as those of Fig. 3. In this regime, the m_3 peak splits into the sub-peaks at $\omega/m_1\approx 2.41$ and 2.65 ($N=22$), indicating that the m_3 peak is broadened intrinsically.

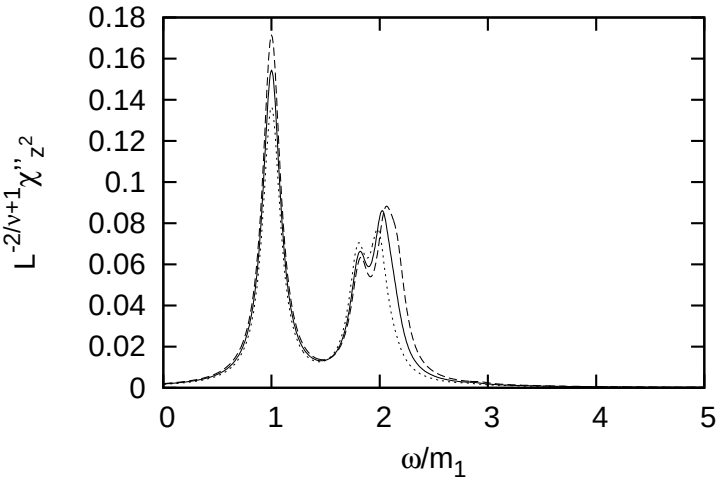

Figure 7: The scaling plot, ω/m_1-$L^{-2/\nu+1}\chi''_{z^2}(\omega)$, is shown with $(D-D_c)L^{1/\nu}=-17$ and $\eta=0.1m_1$ for $N=18$ (dotted), 20 (solid), and 22 (dashed); the scaling parameters, D_c and ν, are the same as those of Fig. 3. The susceptibility χ''_{z^2} is sensitive to the two-magnon continuum extending above $\omega/m_1\geq 2$, which overwhelms the $m_{3,4}$ peaks.

[16] V. Agostini, G. Carlino, M. Caselle, and M. Hasenbusch, Nucl. Phys. B **484** (1997) 331.

[17] R. Fiore, A. Papa, and P. Provero, Phys. Rev. D **67** (2003) 114508.

[18] Y. Nishiyama, Nucl. Phys. B **832** (2010) 605.

[19] M. Hasenbusch, Phys. Rev. B **82** (2010) 174433.

[20] Y. Deng and H. W. J. Blöte, Phys. Rev. E **68** (2003) 036125.

[21] M.A. Novotny, J. Appl. Phys. **67** (1990) 5448.

[22] D. Podolsky, A. Auerbach, and D. P. Arovas, Phys. Rev. B **84** (2011) 174522.

[23] L. Seabra and F. Pollmann, Phys. Rev. B **88** (2013) 125103.

[24] J. A. Kjäll, F. Pollmann and J. E. Moore, Phys. Rev. B **83** (2011) 020407.

[25] N. J. Robinson, F. H. L. Essler, I. Cabrera and R. Coldea, Phys. Rev. B **90** (2014) 174406.

[26] Z. Wang, J. Wu, S. Xu, W. Yang, C. Wu, A. K. Bera, A. T. M. Nazmul Islam, B. Lake, D. Kamenskyi, P. Gogoi, H. Engelkamp, A. Loidl, and J. Deisenhofer, arXiv:1512.01753.

[27] G. Delfino and G. Mussardo, Nucl. Phys. B **455** (1995) 724.